Available online at www.sciencedirect.com
SCIENCE DIRECT®
C. R. Mecanique 332 (2004) 327–343
COMPTES RENDUS MECANIQUE

Microgravity and Transfers/Critical fluids

Equilibration and other dynamic properties of fluids near the liquid–vapor critical point

Horst Meyer [a], Fang Zhong [b]

[a] *Department of Physics, Duke University, Durham, NC 27708, USA*
[b] *Jet Propulsion Laboratory, California Institute of Technology, Pasadena, CA 91109-8099, USA*

Abstract

A review is presented on the advances in understanding equilibration phenomena in compressible pure fluids near the liquid–vapor critical point. The important role of the piston effect is stressed. The equilibration of temperature and density of a fluid sample, kept in a constant volume, are described. Examples are given both above and below the critical point under Earth's gravity (1 g) and microgravity conditions. The good agreement between experimental results and simulations demonstrate the present understanding of the process. The convection onset of a compressible pure fluid in a Rayleigh–Bénard cell at 1 g is described. The impact of the piston effect on the transient, which leads to damped oscillations on the way to reaching a steady state convection, is also described. Here again the results of experiments and numerical simulations are compared. ***To cite this article: H. Meyer, F. Zhong, C. R. Mecanique 332 (2004).***

Résumé

Mise en équilibre et propriétés dynamiques d'un fluide près du point critique liquide–vapeur. Une revue est présentée sur les avancées dans la compréhension des phénomènes de retour à l'équilibre en fluide compressible pur, près du point critique liquide–vapeur. L'accent est mis sur l'importance de l'effet piston. Sont traités le retour à l'équilibre de la température et de la masse volumique d'échantillons à volume constant. Des exemples sont donnés au-dessus et en-dessous du point critique, sous gravité normale (1 g) et en microgravité. Le bon accord entre les résultats expérimentaux et les simulations prouve la validité de la modélisation. Les transitions d'un fluide pur dans une cellule de Rayleigh–Bénard sont décrites sous 1 g. Est étudiée également l'influence de l'effet piston sur la transition qui conduit à la convection stationnaire via des oscillations amorties. Les résultats expérimentaux et ceux des simulations numériques sont comparés dans ce cas également. ***Pour citer cet article : H. Meyer, F. Zhong, C. R. Mecanique 332 (2004).***

Keywords: Fluid mechanics; Supercritical fluid; Equilibration; Piston effect; Microgravity; Rayleigh–Bénard configuration; Convection; Numerical simulation

Mots-clés : Mécanique des fluides ; Fluide supercritique ; Équilibre ; Effet piston ; Microgravité ; Configuration Rayleigh–Bénard ; Instabilité convective ; Simulations numériques

E-mail address: hm@phy.duke.edu (H. Meyer).

1631-0721/$ – see front matter
doi:10.1016/j.crme.2004.02.006

Version française abrégée

Lors d'une conférence internationale en 1989 pour des spécialistes des fluides supercritiques, plusieurs questions fondamentales du comportement dynamique de ces fluides près du point critique (PC) furent discutées, en particulier dans un environnement de microgravité. Cette conférence fut le point de départ d'une initiative rapide vers des réponses à ces questions, tant sur le plan théorique qu'expérimental. Ces efforts furent couronnés de succès comme le montre cette revue.

On récapitule brièvement les deux types d'approches théoriques utilisées pour traiter l'équilibre d'un fluide soumis a une perturbation soudaine, par exemple le changement de température des parois. Sont présentées l'approche thermodynamique [6–8] qui néglige les variations initiales des paramètres sur une échelle de temps acoustique et aussi la vitesse de déplacement, ainsi que l'approche plus complète du groupe de Zappoli [9,11]. Dans cette dernière, l'équation non-linéaire de Navier–Stokes est résolue numériquement pour l'exemple du CO_2, ce qui permet le calcul des propriétés physiques, y compris la vitesse de déplacement, pour des temps comparables et plus grands que l'échelle acoustique. Cette méthode numérique donne une solution très complète du problème sur toutes les échelles de temps. La méthode thermodynamique, plus restreinte, livre cependant des équations plus pratiques à appliquer dans plusieures situations.

On présente d'abord un exemple d'équilibre d'une couche de fluide pur à volume constant, dont les parois horizontales et parallèles ont été assujetties à un changement brusque de température ΔT. Dans ces conditions, des couches limite chaudes sont formées aux deux parois, dont la compression produit un transfert adiabatique rapide d'énergie à travers la couche (Effet piston) menant à une homogénéisation de la température à l'intérieur du fluide. La Fig. 1 montre la configuration expérimentale et les résultats de simulation pour le changement de température δT et de densité $\delta\rho$ pour une couche de ^{3}He avec la valeur moyenne ρ_c, la densité critique. Les variations de δT et $\delta\rho$ sont présentées à plusieurs instants t en fonction de la distance verticale z, (Fig. 1(b), (c)) , et au milieu de la couche en fonction de t (Fig. 1(d), (e)). Cette simulation, faite selon les équations développées dans les références [7] et [8], montre que δT tend vers une valeur d'équilibre bien plus rapidement que si le transfert d'énergie se faisait uniquement par diffusion. Cependant l'équilibre asymptotique de δT, comme celui de $\delta\rho$, se fait de façon diffusive, et devient très lent lorsque l'on s'approche du PC, où le coefficient de diffusion tend vers zéro.

Après la présentation de certaines équations obtenues par la méthode thermodynamique, et la définition des temps caractéristiques « piston » et « diffusif », plusieurs exemples d'équilibre sont présentés. Les résultats expérimentaux sont comparés à ceux des simulations, et le bon accord prouve que le processus est bien compris. Le premier exemple décrit le changement rapide de la température de SF_6 dans une configuration sphérique, Fig. 2 et dans un environnement de microgravité, mesures faites par le groupe de Straub [12]. Dans le deuxième exemple, il s'agit de l'équilibre de la densité dans une couche horizontale de ^{3}He, Fig. 3(a)), et [17], et du temps de relaxation diffusif de la densité, obtenu dans cette série d'équilibres, et porté en fonction de $T - T_c$, Fig. 3(b). Le profil temporel et le temps de relaxation de la température $\Delta T(t)$ à travers la couche fluide lors de l'enclenchement du flux de chaleur, [19], sont présentés sur les Figs. 4(a) et (b).

On décrit une expérience élégante d'équilibre du fluide en dessous du PC avec les phases vapeur et liquide coexistantes et dans des conditions de microgravité, où l'effet piston est responsable de résultats particulièrement spectaculaires, Figs. 5 et 6 et [22,23]. L'exemple final illustre les problèmes rencontrés en présence de ces deux phases pendant des mesures de calorimétrie par le groupe de Straub [3], également en microgravité. Cette recherche, conduite de façon systématique, a présenté la solution du problème, [12]. Ici encore la transmission adiabatique de l'énergie par l'effet piston s'avère importante.

On poursuit cette revue avec le comportement nonlinéaire d'un fluide supercritique, ^{3}He. La convection dans une configuration Rayleigh–Bénard est décrite où $\Delta T(t)$ est encore la différence de température à travers la couche fluide. Dans l'état stationnaire, le profil observé de ΔT en fonction de $T - T_c$ démontre le passage continu du critère de Rayleigh pour le seuil de convection vers celui de Schwarzschild à proximité du PC (Fig. 7 et [30]). Les études expérimentales [30,31,36] et théoriques [32–35] de la variation $\Delta T(t)$ dans le régime transitoire vers l'état de convection stationnaire sont décrites. La Fig. 8 illustre les oscillations atténuées de la température $\Delta T(t)$ après

l'enclenchement du flux de chaleur, observées expérimentalement et obtenues numériquement à 2 dimensions. C'est un phénomène spécial, restreint à un fluide très compressible à volume constant, et non observé dans des fluides communs. La déscription la plus détaillée de la source de ces oscillations, où l'effet piston joue un rôle capital, a été présentée dans [34]. La comparaison des courbes obtenues dans les Fig. 8(a) et (b) témoigne d'un accord raisonnable. La Fig. 9 montre une représentation échelle pour le courant convectif à l'état stationnaire en fonction du nombre de Rayleigh, obtenue pour une gamme de distances $T - T_c$ ou la compressibilité varie dans un facteur 30. La comparaison des observations et des simulations indique un accord satisfaisant. Il en est de même pour les périodes d'oscillation de la température $\Delta T(t)$, dont la représentation échelle est montrée sur la Fig. 10 mais où la loi de puissance avec un exposant $1/2$ demeure à justifier. Malgré ces bons accords, des problèmes importants restent à résoudre aussi bien concernant les observations expérimentales que numériques, et ils sont brièvement mentionnés dans cette revue.

1. Introduction

In March 1989, a small workshop entitled "Equilibration Near the Critical Point" took place at the National Institute of Standards and Technology (NIST) in Gaithersburg, Maryland, USA [1]. The list of participants included experimental and theoretical physicists from several countries with expertise in fluids near the critical point, some of whom had been involved with experiments under microgravity conditions. There were 13 questions to be treated by the participants, such as: "Do we understand the dynamics of equilibration of a one-phase system in the presence of large density and temperature differences?" Intense discussions took place after each presentation in this informal setting. No proceedings of this workshop were produced; however, the organizing committee wrote a report with the perceived response of the participants to the questions treated. Various suggestions and recommendations were made in this report, two of them being the "performance of controlled equilibration experiments in 1-g", and the "performance of calculations employing conventional hydrodynamics and thermodynamics for specific experimental situations, including non-linearity where necessary". The impact of this workshop was strong and rapid: in the following year, papers from several theoretical groups in France, Japan and the USA were published, and several experiments were started, which will be briefly reviewed.

This paper is concerned with pure fluids near their critical point and is divided into two main sections. The first one is a short review of some of the thermodynamic and hydrodynamic predictions for equilibration of a non-convecting fluid layer, and it is followed by a quantitative comparison with experiments. The second is a description of the behavior of a fluid layer subjected to a vertical heat current in a Rayleigh–Bénard cell, both in the convecting steady-state and in the transient stage. The emphasis in the present review is on the description of selected properties and comparison between results from experiments and from numerical calculations for fluids in their transient and their steady state.

We refer to the review by Zappoli [2] on the hydrodynamics of near-critical fluids, where the striking phenomena under conditions of constant volume, such as the 'piston effect' and others are described and explained.

2. Equilibration in the mechanically stable fluid

2.1. Introductory remarks

The 1989 workshop was partly organized to address several unexpected observations in fluid samples near the critical point (CP) during microgravity (μg) experiments and also under normal gravity (1 g) conditions. Among these were: (i) At μg, a much faster temperature response inside bulk fluid SF_6 to a wall temperature change than expected from transport through thermal diffusivity alone [3]; (ii) The failure to observe at the CP the expected sharp peak of the specific heat C_V of SF_6 under μg conditions during the 1985 Spacelab Mission D1 [4];

(iii) A much shorter thermal relaxation time during thermal conductivity measurements in supercritical ^{3}He under 1 g conditions than calculated from the usual Fourier diffusion equation [5]. These problems, and others were discussed at the NIST workshop and the understanding gained there led to rapid theoretical progress and helped to solve these problems within the next few years, as will be described below.

Four papers were published in 1990 describing the treatment of a very compressible pure fluid near its CP, subjected to a sudden temperature change of its container walls. In the work by Onuki et al. [6,7], and by Boukari et al. [8] a purely thermodynamic approach is adopted where the entropy flow equation and mass conservation are used. Here the initial rapid spatio-temporal variations of the pressure on the acoustic time scale that follow the perturbation are neglected, and the pressure is then a function of time only. With the additional assumption of linear hydrodynamics, which implies that only sufficiently small perturbations are considered, the equations of hydrodynamics were shown to reduce to a very simple system of equations for the density ρ, the pressure P, and temperature T which do not contain the flow velocity. In the theory by Zappoli et al. [9], the fully non-linear Navier–Stokes equation is solved numerically for supercritical CO_2, using the Van der Waals equation of state. This second approach permitted the calculation of properties such as velocity, temperature, density, etc., for times comparable and larger than those for the acoustic sound crossing the fluid layer, hence providing information not given by the thermodynamic approach. Finally in the work by Behringer et al. [10], which is based on the thermodynamic equations [7], a calculation of the relaxation process during thermal conductivity measurements eliminates the large discrepancy reported previously between experiments and predictions. In that work, corresponding differential equations for fluid mixtures near the plait point are also derived and the calculated relaxation times are compared with experimental data.

In this review, we will restrict ourselves to the thermodynamic approach, therefore neglecting the rapid variations on the acoustic time scale. Here we briefly recapitulate this approach, which is the starting point for numerical simulations which we compare with experimental results.

2.2. Fluid perturbation: an illustrative example

Before presenting the linearized equations, we describe an experiment in a typical cell, as shown in Fig. 1(a). Here the isothermal horizontal walls at the top and bottom of the fluid layer are kept at the same temperature, $T_{\rm top} = T_{\rm bot}$. By contrast, the vertical walls are thermally poor conductors. The fluid layer has a thickness L and its density ρ has been adjusted close to the critical density ρ_c. This example is for ^{3}He with T_c = 3.318 K, in a cell of $L = 0.2$ cm and average density at the critical density $\rho_c = 0.0414$ g/cm^3. We consider a situation where the fluid is initially in equilibrium $T_{\rm top,bot} = T_0$ with the reduced temperature $\varepsilon \equiv (T_0 - T_c)/T_c = 1 \times 10^{-2}$, and then $T_{\rm top,bot}$ is raised in a step-like manner by an amount ΔT at the time $t = 0$. The magnitude of ΔT is assumed to be small enough, namely $\Delta T \ll T_0 - T_c$, so as to cause negligible changes in the properties of the fluid such as the thermal diffusivity D_T, the thermal conductivity λ, the specific heats C_P, C_V, etc.

Immediately after the step, the fluid in layers adjacent to the horizontal boundaries expands. The formation of boundary layers (light shade in Fig. 1(a)) generates a substantial inhomogeneity in the density distribution in the cell. Under the condition of $V = $ const., the expansion of the boundary layers compresses adiabatically the bulk fluid like moving pistons and this mechanism led to the name of 'piston effect' [9,11], henceforth denoted as PE. In Figs. 1(b) and (c), the spatial profiles of the normalized $\delta T(t, z)$ and $\delta\rho(t, z)$ are shown at several values of t after the step ΔT has been taken. Here $\delta T(t, z) \equiv (T - T_0)$, $\delta\rho(t, z) \equiv (\rho - \rho_c)$, and z is the vertical coordinate.

As a result of the adiabatic compression, the temperature of the bulk fluid approaches the asymptotic value much faster than expected from the diffusive heat propagation alone. The plot in Fig. 1(d) shows the normalized deviations $\delta T_{\rm mid}$ in the middle of the sample versus time. The dashed curve shows for comparison the temperature relaxation predicted by the Fourier diffusion equation. Fig. 1(e) shows the sharp rise of normalized $\delta\rho_{\rm mid}$ due to adiabatic compression and the slow diffusive relaxation to its final value which is the same as the initial one at $t = 0$. The full equilibrium is only achieved after the density inhomogeneity disappears.

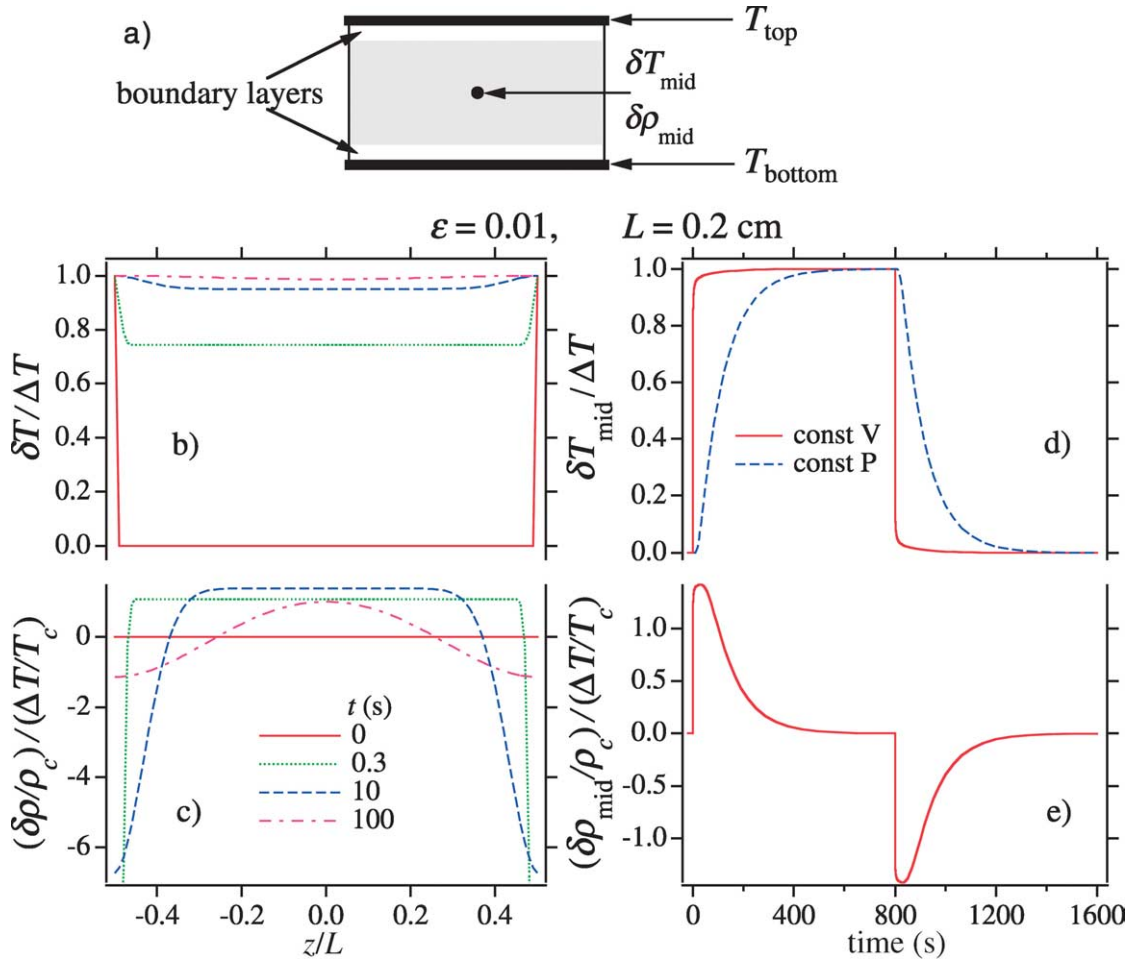

Fig. 1. Illustration of the piston effect mechanism. (a) Schematic fluid cell with height L showing boundary layers (light shade) and bulk fluid (darker shade) with T and ρ sensors in middle. (b) and (c) the spatial distribution of normalized δT and $\delta\rho$ at several time instants t after the initial temperature step ΔT. (d) and (e) time evolutions of the normalized δT and $\delta\rho$ at the cell middle. The experiment is simulated for ^{3}He. For explanations see text.

Fig. 1. Illustration du mécanisme de l'effet piston : (a) vue schématique de la cellule expérimentale pour le fluide, de hauteur L, qui indique les couches limites et le fluide-volumique, avec les sondes de température et de densité au milieu. (b) et (c) distribution spatiale des écarts δT et $\delta\rho$ normalisés à plusieurs instants t après le saut de température initial ΔT. (d) et (e) evolutions temporelles des écarts normalisés δT et $\delta\rho$ au milieu de la cellule. Cette étude est simulée numériquement pour le cas de ^{3}He. Voir le texte pour explications supplémentaires.

When T_{top} and T_{bot} are returned stepwise to their original temperature, i.e., $\Delta T = 0$, at the time $t = 800$ s, the inverse equilibration process takes place. Here the boundary layers are colder than the bulk fluid, leading to a 'cold PE'. They contract and as a result the bulk fluid expands adiabatically, hence the density shows a sharp negative peak and then relaxes diffusively to its original equilibrium value.

The response of the bulk fluid to the temperature change at the horizontal walls explains the apparent 'fast' temperature equilibration in the calorimeter of Nitsche and Straub [3], as we will describe below with more details. We emphasize that although in the asymptotic regime the amplitudes of the exponential terms for δT and $\delta\rho$ are different, both quantities are still relaxing exponentially to equilibrium with the same time constant τ_0. The 'critical speeding up' due to the PE does not make the asymptotic rate of the temperature equilibration faster than that of $\delta\rho$,

it only dramatically reduces the fraction of the total temperature change that equilibrates exponentially. Hence the uniformity of the fluid temperature – strikingly demonstrated in recent experiments [12] – is not a good indicator of how close the system is to equilibrium, because in a very compressible fluid one can have non-equilibrium densities with almost homogeneous temperature distribution.

2.3. Transport equations in the supercritical fluid, experiments and simulations

First we recapitulate the governing equations and describe three different sets of experiments where the results are compared with numerical simulations. For the following conditions: (a) pure fluid in one phase; (b) constant volume; and (c) negligible gravity effects, Boukari et al. [8], starting from the equation for energy conservation, obtained. Then

$$\frac{\partial \delta T}{\partial t} = \alpha \left(\frac{\partial \delta T}{\partial P} \right)_{\rho} \frac{\partial \delta P}{\partial t} + \frac{1}{\rho C_P} \nabla (\lambda \nabla \delta T) \tag{1}$$

Here $\delta P = P - P_0$, where P_0 is the initial equilibrium value. Also $\alpha \equiv [1 - \frac{1}{\gamma}]$, where $\gamma \equiv C_P/C_V$, and λ is the thermal conductivity. From this equation and the mass conservation relation, the evolution of the fluid system can be calculated. From the theoretical work of Boukari et al. [13], it appears that the fluid velocity during the equilibration transient is small enough that it can be neglected, therefore justifying the approximation made in deriving the equation above.

The Onuki–Ferrell approximations [7] lead to the equations listed below for the same conditions as above and also for small enough perturbations (such as $\Delta T \ll T - T_c$). The linearized equations in 1D are then

$$\frac{\partial \delta T}{\partial t} = \alpha \frac{\partial \langle \delta T \rangle}{\partial t} + D_T \frac{\partial^2 \delta T}{\partial z^2} \tag{2}$$

$$\delta \rho = \left(\frac{\partial \rho}{\partial T} \right)_P \big(\delta T - \langle \delta T \rangle \big) \tag{3}$$

$$\delta P = \left(\frac{\partial P}{\partial T} \right)_{\rho} \langle \delta T \rangle \tag{4}$$

Here the brackets $\langle \cdots \rangle$ denote averaging over the fluid volume, and $D_T = \lambda/\rho C_P$ is the thermal diffusivity. If the fluid is incompressible, $\gamma = 1$ and Eqs. (1) and (2) reduce to the Fourier equation.

Consider a very compressible fluid where $\gamma \gg 1$, and use the linearized 1D equations. The temperature change in the bulk fluid shortly after the step change ΔT is [7]

$$\delta T(t) \propto (t/t_1)^{1/2} \tag{5}$$

where the characteristic 'piston time' $t_1 = L^2/4\gamma^2 D_T$. From the critical behavior of $\gamma \propto \varepsilon^{-1.2}$ and $D_T \propto \varepsilon^{0.63}$, it follows that $t_1 \to 0$ as the CP is approached. At long times $t > \gamma^2 t_1$, the final equilibrium value is approached exponentially as

$$\Delta T - \delta T(t) \propto \exp[-t/\tau_0] \tag{6}$$

with the slowest mode relaxation time $\tau_0 = L^2/4\pi^2 D_T$ ($\gamma \gg 1$). As γ decreases, the ratio $\tau_0/(\frac{L^2}{4\pi^2 D_T})$ increases from 1 to 4. Hence for an incompressible fluid, the relaxation time for the same value of L and D_T is 4 times longer than for a very compressible one [10].

We first deal with the experiments where the temperature change was measured. In early equilibration experiments following the 1989 workshop, the 'critical speeding up' of the temperature response to a change in the wall temperatures was demonstrated at 1 g [14] and under μg conditions [15]. Straub et al. [12] carried out experiments in a spherical cell of 20 mm diameter filled with SF_6 at the critical density both under μg and also 1-g conditions. Here $T_c = 318.72$ K, $P_c = 3.75$ MPa, and $\rho_c = 0.742$ g/cm^3. The cell was subjected to a heat pulse

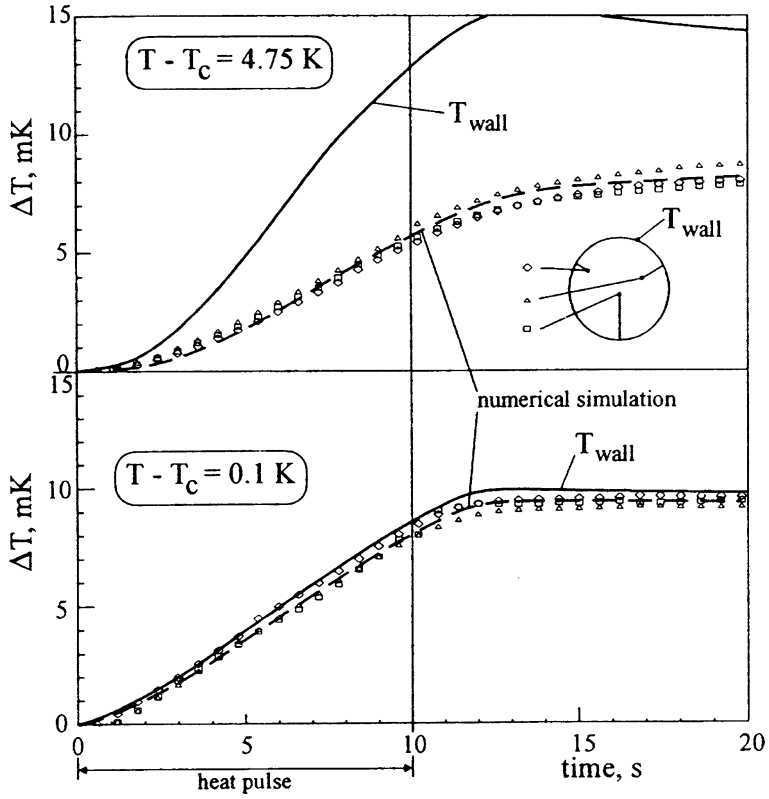

Fig. 2. Experiment by Straub et al. [12]: comparison of two typical temperature response runs above T_c under μg conditions. The changes of δT in the fluid, measured by three sensors positioned as shown, are given by symbols. The solid line represents T_{wall} and the dashed line the numerical simulations. (Reprinted with kind permission from Kluwer Academic Publishers.)

Fig. 2. Expériences de Straub et al. [12] : comparaison de deux mesures de température typiques au dessus de T_c en μg. Les changements de δT dans le fluide, mesurés par les trois sondes placées comme indiqué sur le croquis, sont marqués par des symboles. Les lignes continues représentent T_{wall}, la température de paroi, et les pointillés les simulations numériques. (Re-publié avec la permission de Kluwer Academic Publishers.)

of constant power for a duration of 10 s and the temperature was monitored on the cell wall and at three positions inside the cell. In Fig. 2 the temperature response is shown at two temperatures, $T - T_c = 4.74$ K and 0.1 K under microgravity conditions. Here the symbols indicate the temperature measured at the various locations inside the fluid, the solid line represents the T_{wall} profile and the dashed curve is the result of numerical simulation from the equations of Boukari et al. [8], and in consideration of the spherical shape of the sample cell. The results show clearly how the energy transfer improves as the CP is approached. For $T - T_c = 0.1$ K, the temperature in various places of the fluid follows very closely that of the wall. This is quite in contrast with what one would expect if the energy transfer was by diffusion only, which becomes a very slow process as the CP is approached.

Next we describe the local density changes measured with fluid ^{3}He under 1-g condition. The experiments were carried out along the critical isochore in a cylindrical cell schematically shown in Fig. 1(a), where again both T_{top} and T_{bot} were raised stepwise by ΔT then, after a time interval, returned stepwise to their original value. The fluid layer had a diameter of 19.1 mm and a height $L = 3.5$ mm. Inside the cell, capacitive density sensors were placed each approximately at $L/3$ from the top and bottom plates. The purpose of having two sensors was to probe the effect of stratification on the density response for various values of ε. In the two-phase regime below T_c, the sensors then measured the vapor and the liquid density respectively. The first such experiments

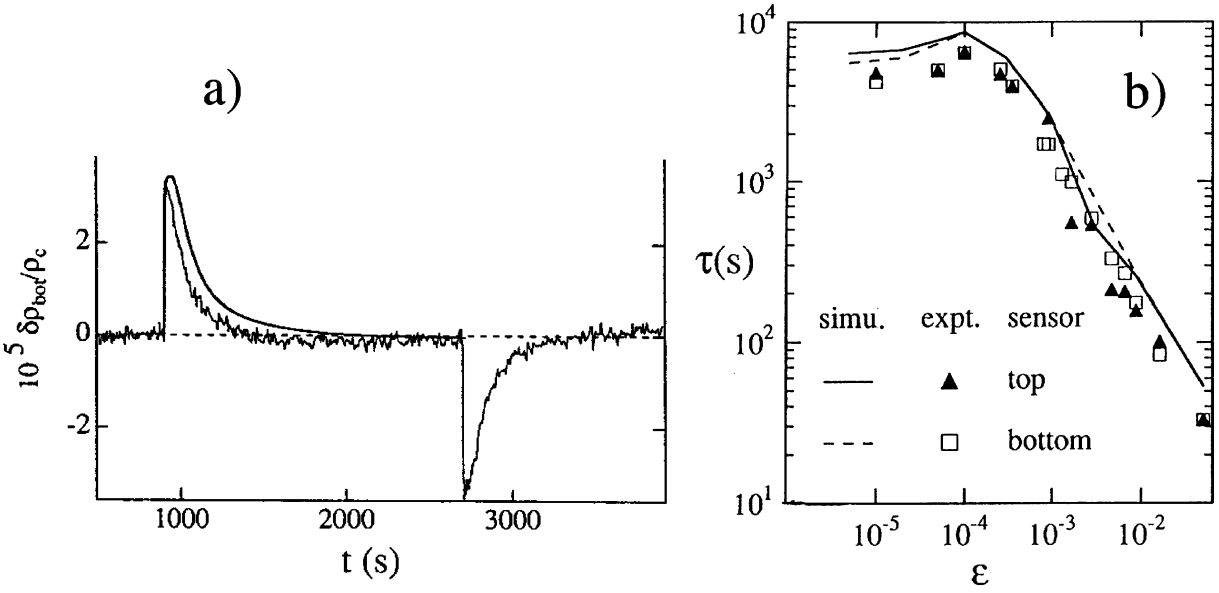

Fig. 3. (a) The normalized density change $\delta\rho(t)$ at the lower sensor in supercritical ^{3}He after a temperature step $\Delta T = 80$ μK, and a stepwise return to $\Delta T = 0$. Measurements were taken at $T - T_c = 29$ mK ($\varepsilon = 8.8 \times 10^{-3}$). (b) The relaxation time τ of the density change $\delta\rho(t)$ as a function of ε. Symbols: data as measured with the upper and lower sensors. Solid and dashed lines: calculations.

Fig. 3. (a) Le changement normalisé de la densité $\delta\rho(t)$ enregistré par la sonde inférieure dans l'échantillon de ^{3}He supercritique après un saut de température $\Delta T = 80$ μK et un retour similaire à $\Delta T = 0$. Les mesures ont été faites à $T - T_c = 29$ mK ($\varepsilon = 8{,}8 \times 10^{-3}$). (b) Le temps de relaxation τ du changement de densité $\delta\rho(t)$ en fonction de ε. Symboles : résultats obtenus avec les sondes supérieure et inférieure. Lignes continues et pointillés : calculs.

were carried out as described in [16]. More recent experiments [17] in a cell with improved construction and suspension of the sensors gave the same qualitative results as in [16], but the data agreed better with the numerical simulations using Eqs. (2) and (3). The temporal profiles of both experiment and simulation for the lower density sensor are shown in Fig. 3(a). Here the temperature steps were ±80 μK with initial temperature $T - T_c = 29$ mK ($\varepsilon = 8.8 \times 10^{-3}$). For comparison, the piston time $t_1 = 0.16$ s and the relaxation time for the slowest mode is $\tau_0 = 330$ s. In Fig. 3(b) we show the measured relaxation times τ above the CP at 1 g, compared with predictions from numerical simulations. There is good agreement between prediction and experiment, considering that the experimental cell is more complicated than the ideal one used in the calculations. As a result, the effective height L of the cell is smaller than the nominal one, which causes a systematic displacement of the experimental data to lower values of τ respectively to the simulations. As ε decreases, τ passes over a maximum and tends to a constant value. This behavior for $\varepsilon < 10^{-3}$ is due to the stratification where the density of the fluid is off the critical isochore. The result is that the average $\langle D_T \rangle$ over the fluid sample is larger than it would be along the critical isochore, and this causes a corresponding decrease in τ. In the absence of gravity, τ would have continued the upwards trend, diverging as $\varepsilon \to 0$.

The thermal response of supercritical ^{3}He along the critical isochore has also been studied when the fluid was subjected to periodic temperature oscillations of the top and bottom walls of the cell [18]. The experiments were carried out at frequencies between 4×10^{-4} and 2 Hz, and at several values of ε. Comparison was made with calculations based on the Onuki–Ferrell linearized equations. There was good agreement, but again with a systematic shift of the experiments respectively to the calculations, reflecting the differences in the effective height L between the experimental and the ideal cell used in the calculations, as was mentioned before. This experiment provided a different approach in the study of the PE in the fluid and corresponds to a Fourier transform

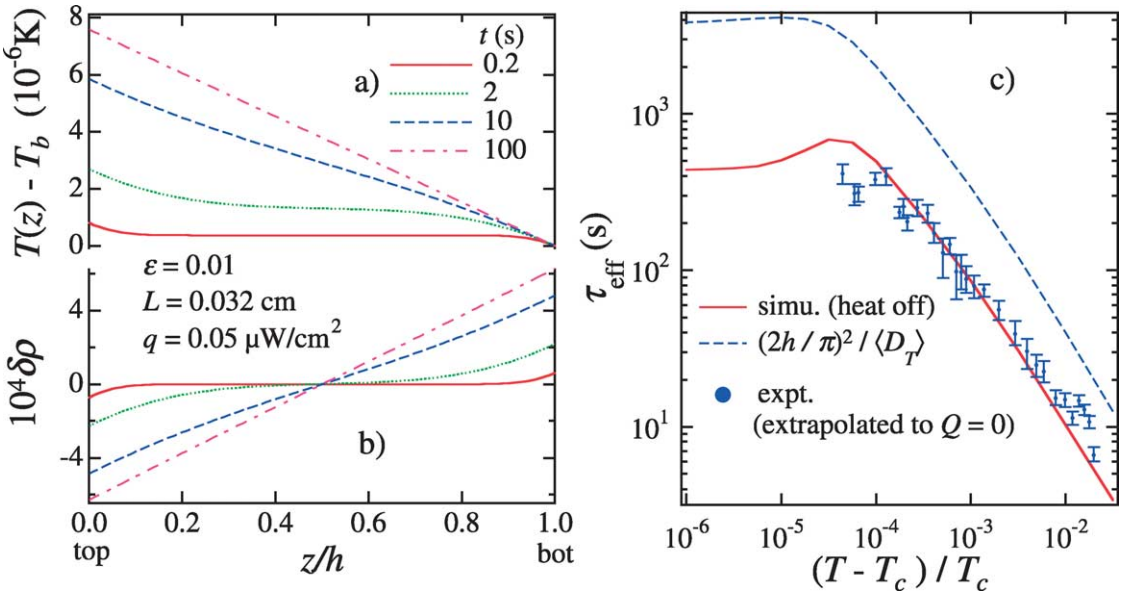

Fig. 4. Thermal conductivity experiment: spatial profiles of (a) $\delta T(z,t)$ and (b) $\delta\rho(z,t)$ for ^{3}He at $\rho = \rho_c$ at several times t after the start of the constant heat current q. (c) The relaxation time τ_{eff} for ^{3}He in the heat conductivity cell, as measured by the equilibration of $\delta T(t)$ for the cell with $L = 0.032$ cm. Symbols: experimental data. Solid line: relaxation time obtained from the simulation of Eq. (1) in 1 g [19]. Dashed line: initial calculations [5] where the Fourier equation ($\gamma = 1$) was used.

Fig. 4. Mesures de conductivité thermique : profils spatiaux : (a) $\delta T(z,t)$ et (b) et $\delta\rho(z,t)$ pour ^{3}He avec $\rho = \rho_c$ à plusieurs instants t après l'enclenchement du flux de chaleur constant q. (c) Temps de relaxation τ_{eff} pour ^{3}He dans la cellule expérimentale, mesure par la mise à l'équilibre de $\delta T(t)$ pour une hauteur de fluide $L = 0{,}032$ cm. Symboles : résultats expérimentaux. Ligne solide : temps de relaxation obtenus à partir des simulations de l'Éq. (1) sous gravité normale [19]. Ligne pointillée : les calculs initiaux [5] en utilisant l'équation de Fourier avec $\gamma = 1$.

where the time scale is replaced by the frequency. It explores the density response at times as short as 0.1 s, much shorter than a step-change ΔT of the boundary temperature is able to do.

We now discuss the heat transport and thermal relaxation during thermal conductivity measurements. The fluid layer was contained in a cell between two horizontal plates such as in Fig. 1(a). Initially the fluid is in equilibrium at a temperature T_0. A constant heating power q is applied to the top plate while the lower plate is kept at $T_{\text{bot}} = T_0$. As a result its temperature T_{top} rises until a steady temperature $T_{\text{top}}(\infty)$ is reached. The fluid always remains mechanically stable. From the ratio $[T_{\text{top}}(\infty) - T_0]/q$ the effective thermal conductivity λ is derived. The temporal and spatial profiles of $\delta T(t,z)$ and $\delta\rho(t,z)$ can again be obtained from Eqs. (2) and (3) but with different boundary conditions than those used for Fig. 1(a). The spatial profiles [19] are shown in Fig. 4(a), (b) and are to be compared with those of Fig. 1(b), (c). Boundary layers are again formed, namely a 'hot' layer at the top and a 'cold' one at the bottom. The PE homogenizes the temperature of the bulk fluid which rises with time. The space where δT is homogeneous shrinks as the boundary layer width increases. Finally in the steady-state there is a quasi-linear temperature drop across the fluid layer. The PE also accelerates the transient to reach the steady state. Both the initial slope $\partial T_{\text{top}}(t)/\partial t$ is steeper and the relaxation time τ_0 is shorter than for a diffusive process alone. A similar figure was obtained by Zappoli et al. (Fig. 5 of [9]). In that simulation T_{top} was raised stepwise by ΔT, while T_{bot} was kept constant. In that case the initial temperature gradients in the boundary layer are much sharper than presented in Fig. 4(a) where different boundary conditions were used.

Fig. 4(c) shows the relaxation time in ^{3}He along the critical isochore where the symbols are the experiments and the dashed curve is the initial calculation [5] starting from the diffusive Fourier equation. The large discrepancy is

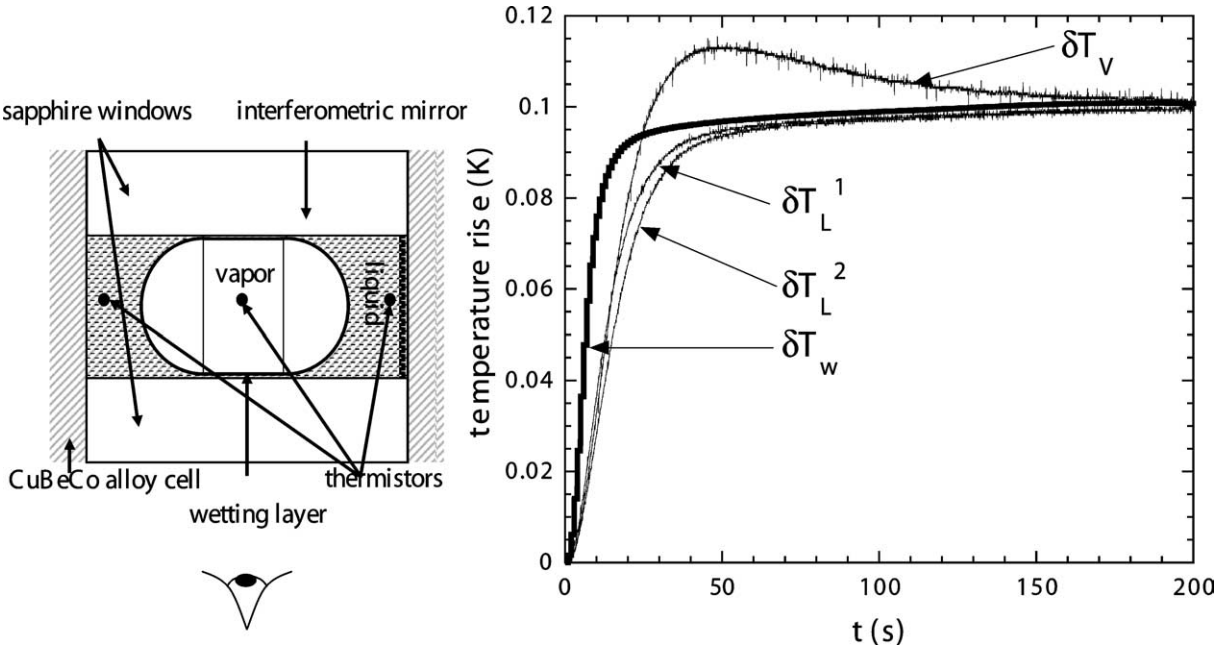

Fig. 5. Left side: schematic cross-section of the experimental cell in [22] filled with fluid in the coexisting phase regime under µg conditions, showing the location of the thermistors inside the interferometric cell. The hatched space around the vapor bubble is the liquid. Right side: temperature rise measurements: δT_W is the cell wall. The top curve δT_V is the vapor response, while δT_L^1 and δT_L^2 are the responses of the sensors in the liquid, located as in Fig. 6(a).

Fig. 5. Côte gauche : section droite schématique de la cellule expérimentale [22] avec un fluide en régime de phases coexistantes sous conditions de µg, gui indiquent la position des thermistors dans la cellule interférométrique. L'espace hachuré autour de la bulle de vapeur est le liquide. Côté droit : mesures de l'augmentation de température : δT_W est mesuré sur la paroi de la cellule. La courbe supérieure δT_V décrit la phase vapeur, tandis que δT_L^1 et δT_L^2 représentent la réponse des sondes dans la phase liquide, et qui sont situées comme indiqué dans Fig. 6(a).

suppressed by use of Eq. (2) [10]. Further improvement in the agreement was obtained from a new data analysis and numerical simulation [19] shown by the solid line.

Finally, we mention the very careful and accurate equilibration experiments in supercritical SF_6 under µg conditions [20]. Here interferometry was used to measure the density changes associated from the late stage of thermal equilibration in a flat cylindrical fluid layer. From these measurements and the analysis which used Eq. (2), the range of D_T data could be extended to temperatures as close as $T - T_c = 0.0015$ K (or $\varepsilon = 5 \times 10^{-6}$!), and they agreed well with other measurements with which they overlapped at $T - T_c > 0.07$ K.

2.4. Experiments and numerical calculations below CP

The description of equilibration in the two-phase regime below the CP is obtained by an extension of the equations described above. Onuki and Ferrell [7] have discussed several aspects of the equilibration processes, and relevant equations were developed for simulations which were carried out for ^{3}He [21]. Because of their complexity, they will not be presented here. The existence of the interface between liquid and vapor introduces a bottleneck in the heat transfer between the two phases, which has been shown to slow down the process of equilibration, as discussed in [7,10].

Data and their analysis have been reported for several experiments in both microgravity and 1 g conditions, and we restrict our discussion to two particularly interesting examples. The first one is a very elegant experiment with SF_6 carried out by Wunenburger et al. [22], for which the results were subsequently compared with numerical

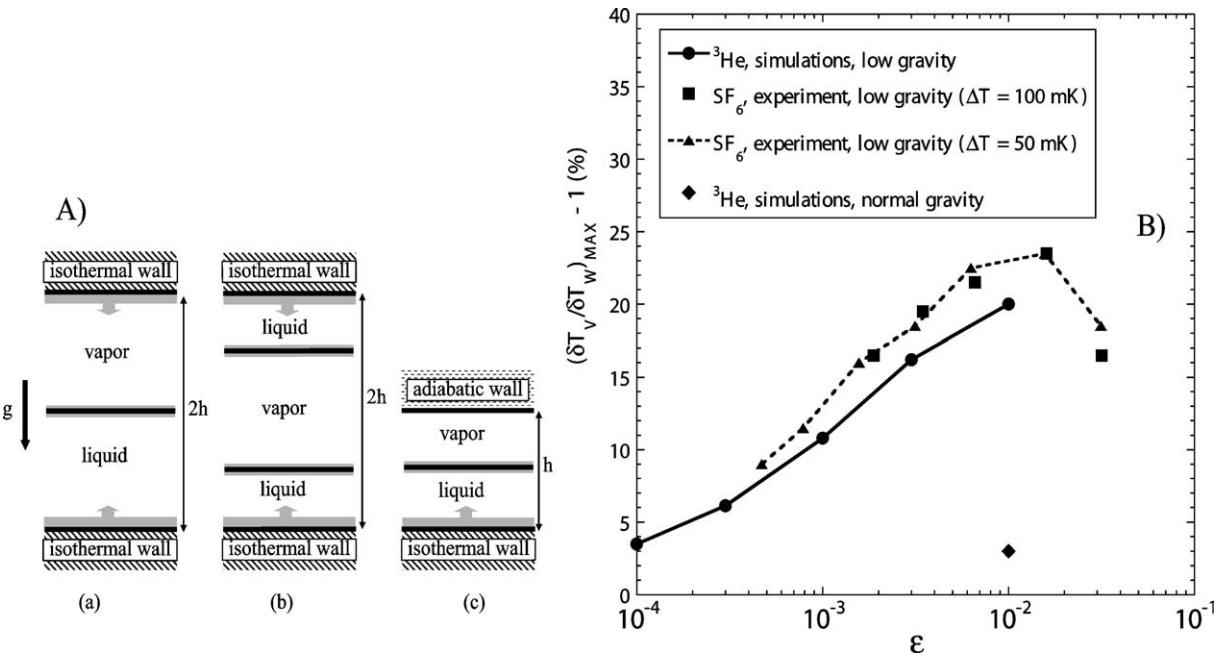

Fig. 6. (A) 1D sketch of liquid and vapor phase distribution at (a) 1 g and (b) µg. (c) 1D cell and phase distribution equivalent to (b), as used in simulations (from [23]). (B) Comparison between measured vapor overheating in SF_6 and simulations in ^{3}He. Solid triangles and squares: maximum reduced overheating observed ($\delta T_V/\Delta T_W$) observed in SF_6 for $\Delta T = 50$ and 100 mK. Solid circles and line: maximum reduced ^{3}He vapor overheating ($\delta T_V/\Delta T_W$), computed numerically, with the vapor isolated from the thermostated cell (Fig. 6(A(c))). Diamond: maximum reduced overheating computed with the vapor in contact with thermostated cell (Fig. 6(A(a))).

Fig. 6. (A) Croquis à une dimension de la distribution des phases liquide et vapeur sous conditions (a) 1 g et (b) µg. (c) Cellule à une dimension et distribution de phase equivalente à (b), qui est utilisée dans les simulations (d'après [23]). (B) Comparaison du surchauffage de la vapeur dans SF_6 avec les simulations dans ^{3}He. Triangles et carrés : surchauffage maximum en représentation réduite observé avec SF_6 pour $\Delta T = 50$ et 100 mK sous condition de microgravité (selon croquis 6(A(b))). Cercles noirs et courbe : surchauffage maximum de la vapeur de ^{3}He ($\delta T_V/\Delta T_W$), par méthode numérique, la vapeur étant isolée thermiquement de la paroi (selon croquis Fig. 6(A(c))). Losange noir : surchauffage maximum calculé numériquement, la vapeur étant en contact thermique avec la paroi thermostatée de la cellule.

simulations on ^{3}He [23]. In the experiment, the temperature responses of the two coexisting phases of vapor and liquid were measured after a temperature increase from an equilibrium state. The experimental cell had windows for observing interferometrically the vapor phase with the shape of an ellipsoidal bubble and the liquid phase surrounding it and wetting the walls. There were also three sensors probing the temperature of the two phases, T_V and T_L, as shown in Fig. 5(left). When the cell wall temperature T_W was changed from $T = T_c - 10.1$ K by a step of $\Delta T = +100$ mK, the sensors in the liquid phase showed a rapid temperature increase and tended from below to the asymptotic T_W. However the vapor temperature T_V overshot T_W by a considerable amount before approaching it from above, as shown in Fig. 5(right). This overheating phenomenon results from the inhomogeneous adiabatic energy transfer process in the two-phase regime, where the bubble is thermally insulated from the thermostated walls by the liquid phase. Such an effect, although with much smaller amplitude, was already simulated for ^{3}He in 1 g where the vapor occupies the upper portion of the cell and without the thermal insulation from the top wall [21]. Fig. 6 shows a comparison in a reduced representation between the experiments with SF_6 and the simulations with ^{3}He, which shows good consistency. For the simulations in 0 g, an adiabatic wall was substituted in the middle of the vapor space, as illustrated in Figs. 6 (b) and (c) to create the thermal insulation from the wall. For the simulations at 1 g, see solid diamond in Fig. 6(a). The authors of [23] have also presented a discussion of the initial observed ratios $(\delta T_V/\delta T_W)_{\max}$ as compared with predictions by Onuki and Ferrell [7].

The second example illustrates the problems that can be encountered in reaching an equilibrium state in the two-phase regime, and is given by the calorimetry experiments by the group of Straub. In their initial C_V measurements of SF_6 for $\rho = \rho_c$ at μg [3], the sample was continuously heated from the lowest temperatures below the CP into the homogeneous phase. Experiments at comparable slow ramp rates were internally inconsistent and the expected sharp peak in C_V was not observed, in contrast to measurements at 1 g. Obviously the fluid system had not reached equilibrium during the temperature ramping in μg conditions, where convection was not available to help improving the equilibration rate. This phenomenon was subsequently explained in detail by Straub et al. [12]. Using a temperature-entropy diagram, the effect of heating and cooling the sample in the two-phase region was elaborated. The authors pointed out that, in contrast to heating, cooling produces a rapid exchange of mass and heat between the two phases by isentropic expansion leading to the nucleation of bubbles in the liquid phase and droplets in the vapor phase. Because of the latent heat consumed (respectively released) by the subsequent growth of these bubbles and droplets, the surrounding fluid returns quickly to saturation condition. As a result, the two-phase system, when cooled at a slow enough rate, is always close to its equilibrium state, in contrast to the heating process. This explains the strong hysteresis in the C_V data, where those obtained by cooling showed the expected singularity and permitted reproducible measurements which led to an accurate determination of the critical exponent α and the leading amplitude [4,24]. The cell used in these measurements was the same – a 20 mm diameter spherical shell – as in the investigation of the temperature propagation described above [12].

3. Non-linear hydrodynamics: the transient to convection and early turbulence

In this section we describe how the large compressibility characteristic of supercritical fluids affects the onset of non-linear behavior, namely the transient to convection and turbulence. Again the emphasis is on comparing experiments with predictions and simulations. A review of the hydrodynamic instabilities with a number of references has been presented in the article by Zappoli [2].

Here we consider the heat transport processes in a Rayleigh–Bénard cell (RB), with a horizontal fluid layer between two isothermal plates, as shown schematically in Fig. 1(a). Here $T_{\text{top}} = T_0$ is kept constant and the bottom plate with T_{bot} is initially at the same equilibrium temperature. The application of heating power q to the bottom plate produces an increase $\delta T(t) = T_{\text{bot}} - T_0$ across the fluid layer with a steady-state value of $\Delta T = \delta T(t = \infty)$, which is a function of ε and q. To predict the onset of mechanical instability, usually given by the Rayleigh criterion for incompressible fluids, the compressibility needs to be taken into account. This problem was first solved by Gitterman and Steinberg [25] (GS), and more recently a much simpler form for the transition function $\Delta T_{\text{onset}}(\varepsilon)$ was obtained by Carlès and Ugurtas [26] (CU), which gives almost identical numerical results as those from [25]. The transition curve is then given by $\Delta T(\varepsilon)_{\text{onset}} = \Delta T_{\text{Ra}} + \Delta T_{\text{ad}}$, where $\Delta T_{\text{Ra}} = Ra_c \times (D_T \eta / \rho g \alpha_P L^3)$, the Rayleigh criterion [27], and $\Delta T_{\text{ad}} = \rho L g (1 - C_P/C_V)(\partial T/\partial P)_\rho$, the term from the Schwarzschild criterion [28]. Here $Ra_c = 1708$ is the critical Rayleigh number for a cell with a large enough aspect ratio (in practice > 5 [29]), η is the shear viscosity, and α_P is the coefficient of isobaric thermal expansion. As α_P/D_T diverges when the CP is approached, $\Delta T_{\text{Ra}} \to 0$. The term ΔT_{ad} predicts the stability limit from the adiabatic temperature gradient [27], and in contrast to the Rayleigh term, ΔT_{ad} increases slowly and tends to a constant value as the CP is approached. Because the dependence on L is quite different for the two terms, the resulting $\Delta T(\varepsilon)_{\text{onset}}$ has a shape that is a strong function of L. For studies of convection with ^{3}He, a layer thickness $L = 0.1$ cm offers the possibility of studying the crossover between the two asymptotic regimes over a convenient range of ε. For $\varepsilon > 0.1$, ΔT_{Ra} dominates while for $\varepsilon < 0.01$ it is insignificant relative to ΔT_{ad}. Fig. 7 shows both the experimental data and the calculated curve [30], where the agreement is satisfactory even close to the CP where the transition could not be sharply defined by the experiments. The small value of $\Delta T_{\text{onset}} = 3.6$ μK near CP for $L = 0.1$ cm compares with ΔT_{onset} of a few mK for a much less compressible fluid such as liquid ^{3}He or ^{4}He at saturated vapor pressure at temperatures well below the critical point, also for $L = 0.1$ cm (see Fig. 4(a) in [29]).

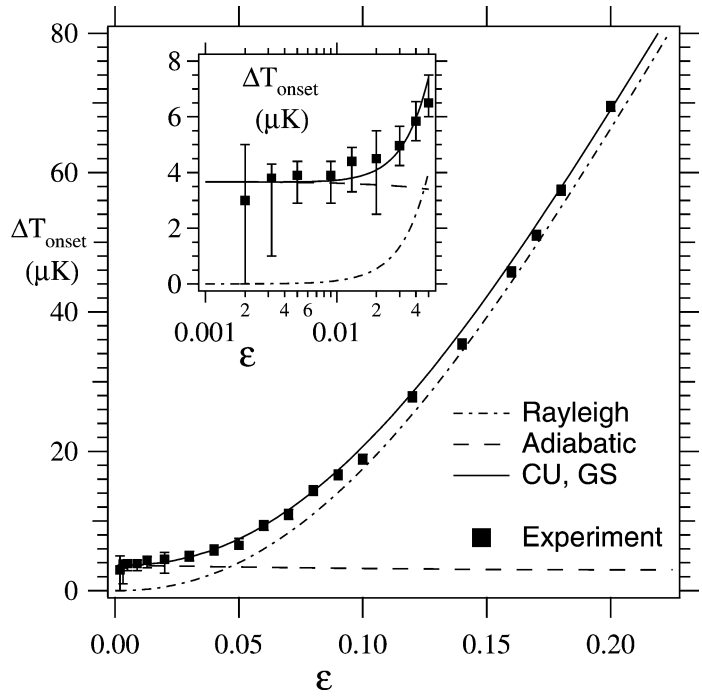

Fig. 7. Comparison of the experimentally détermined ΔT_{onset} versus ε (symbols) with theory (lines) by CU and GS. Main figure: linear plot. Inset: semilogarithmic plot in the region where the term ΔT_{ad} is dominant. The 'error bars' represent the approximate width of the transition. (Figure initially published by the American Physical Society.)

Fig. 7. Comparaison de $\Delta T_{\text{onset}}(\varepsilon)$, determiné expérimentalement (symboles) avec les prédictions théoriques de CU et GS (courbes). Figure principale : échelle linéaire. Figure intérieure : échelle semi-logarithmique dans la région ou ΔT_{ad} domine. Les barres verticales représentent la largeur approximative de la transition. (La figure initialement publiée par l'American Physical Society.)

Generally a compressible fluid does not satisfy the criteria of the Boussinesq approximation which simplify the hydrodynamic equations. However it can be shown that by suitably correcting the Rayleigh and Nusselt number as shown below, the set of Boussinesq criteria is recovered [28]. This is discussed in [30]. One then obtains

$$Ra_{\text{corr}} = Ra\frac{(\Delta T - \Delta T_{\text{ad}})}{\Delta T}, \qquad Nu_{\text{corr}} = \frac{(\Delta T^{\text{diff}} - \Delta T_{\text{ad}})}{(\Delta T - \Delta T_{\text{ad}})} \tag{7}$$

where $Ra = \alpha_P \rho g L^3 \Delta T/\eta D_T$. Also ΔT^{diff} is the temperature drop across the fluid in the diffusive regime for the same heat current q that produces the observed steady-state ΔT. Because α_P/D_T strongly diverges as the CP is approached, Ra_{corr} numbers of the order of 10^8 can be obtained for ΔT only a few tens of μK above the convection onset for a cell with $L = 0.1$ cm, and where the Boussinesq criteria are still satisfied.

The transient to steady state convection after starting a constant heat current q across the fluid layer in a RB cell has received the attention from several groups. In their numerical simulations, Amiroudine and Zappoli [34] have used the complete Navier–Stokes (NS) equation together with the enthalpy equation, where the piston effect is implicitly taken into account in the pressure force term. In the simulations by Furukawa and Onuki [33] a simplified NS equation was used and the piston effect was taken into account by the modified linearized energy equation, Eq. (2), where a term from the gravity field was introduced. For small enough Ra_{corr}, the Stokes approximation was made for the NS equation [32]. Although these two approaches are quite different, similar numerical results were obtained, as will be seen below. Furthermore El Khouri and Carlès [35] have calculated the instability onset of a ^{3}He layer in a RB cell and determined the initial convection modes under different scenarios of ε and q.

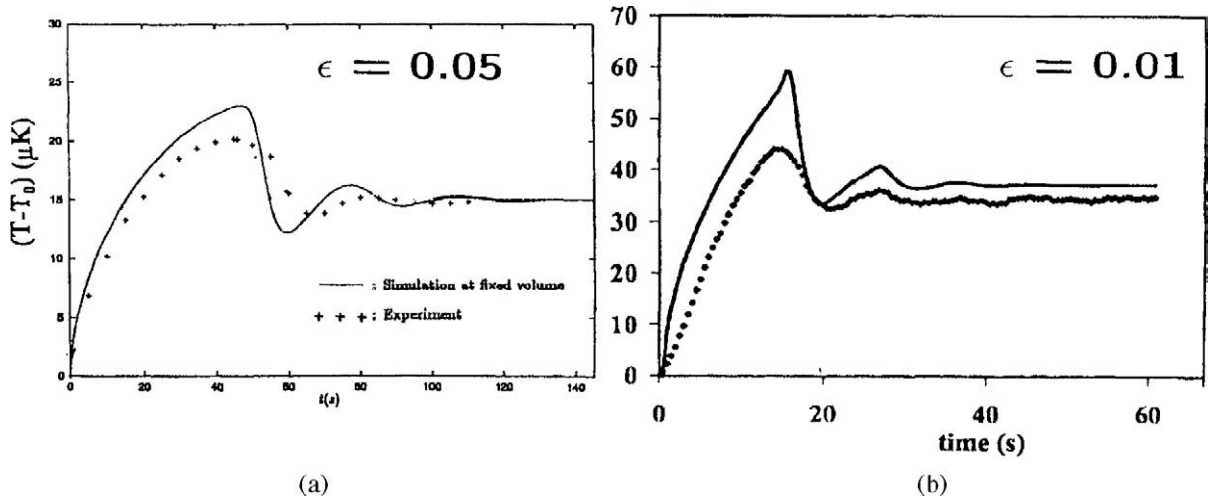

Fig. 8. Representative profiles $\Delta T(t)$ in supercritical ^{3}He from experiments (symbols, or noisy curve) and from simulations (solid curve): (a) $\varepsilon = 0.05$ from [32]; (b) $\varepsilon = 0.01$ from [34]. (Reprinted with permission of the authors; originally published by the American Physical Society.)

Fig. 8. Profiles représentatifs $\Delta T(t)$ dans le ^{3}He supercritique, obtenus à partir des mesures (symboles ou courbe avec bruit de fond) et des calculs numériques (courbe solide) : (a) $\varepsilon = 0{,}05$, d'après [32] ; (b) $\varepsilon = 0{,}01$ d'après [34]. (Re-publié avec la permission des auteurs ; initialement publié par l'American Physical Society.)

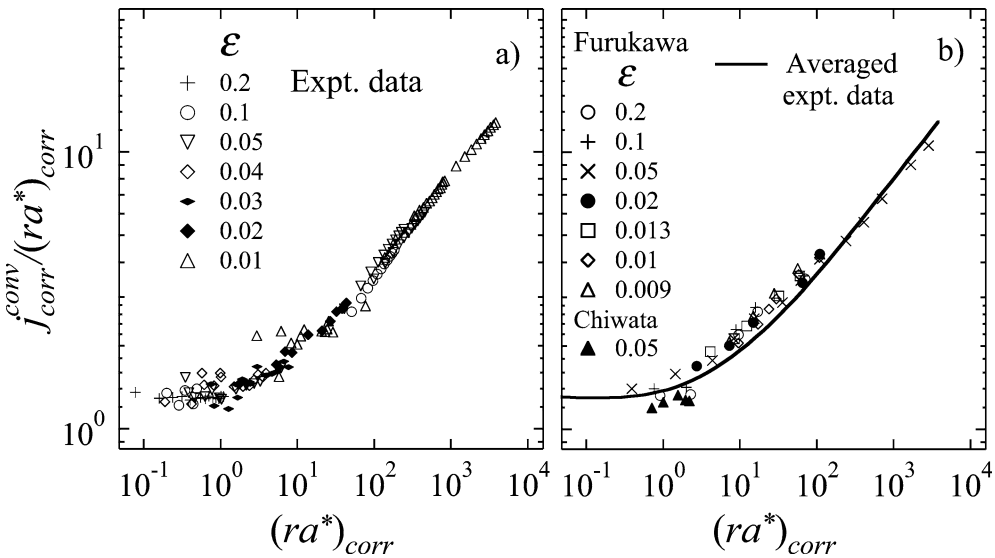

Fig. 9. The convective heat current $j^{\text{conv}}_{\text{corr}}$ divided by ra^*_{corr}, the reduced Rayleigh number $ra^*_{\text{corr}} = [Ra_{\text{corr}} - Ra_c]/Ra_c$, plotted versus ra^*_{corr}. Both are corrected for the adiabatic temperature gradient contribution, as explained in the text. (a) Experimental data at various values of ε. (b) Data from simulations at different values of ε shown by symbols. The solid line is the average of the experimental data in Fig. 9(a). Taken from [36]. (Figure initially published by the American Physical Society.)

Fig. 9. Le courant convectif $j^{\text{conv}}_{\text{corr}}$ divisé par ra^*_{corr}, le nombre de Rayleigh réduit $ra^*_{\text{corr}} = [Ra_{\text{corr}} - Ra_c]/Ra_c$, représenté en fonction de ra^*_{corr}. Ces deux paramètres sont corrigés en tenant compte du gradient adiabatique de température, comme expliqué dans le texte. (a) Résultats expérimentaux pour plusieurs valeurs de ε. (b) Résultats obtenus par les simulations numériques pour plusieurs valeurs de ε, indiqués par des symboles. La courbe continue est la moyenne des résultats expérimentaux (Fig. 9(a)). D'après [36]. (Figure initialement publiée par l'American Physical Society.)

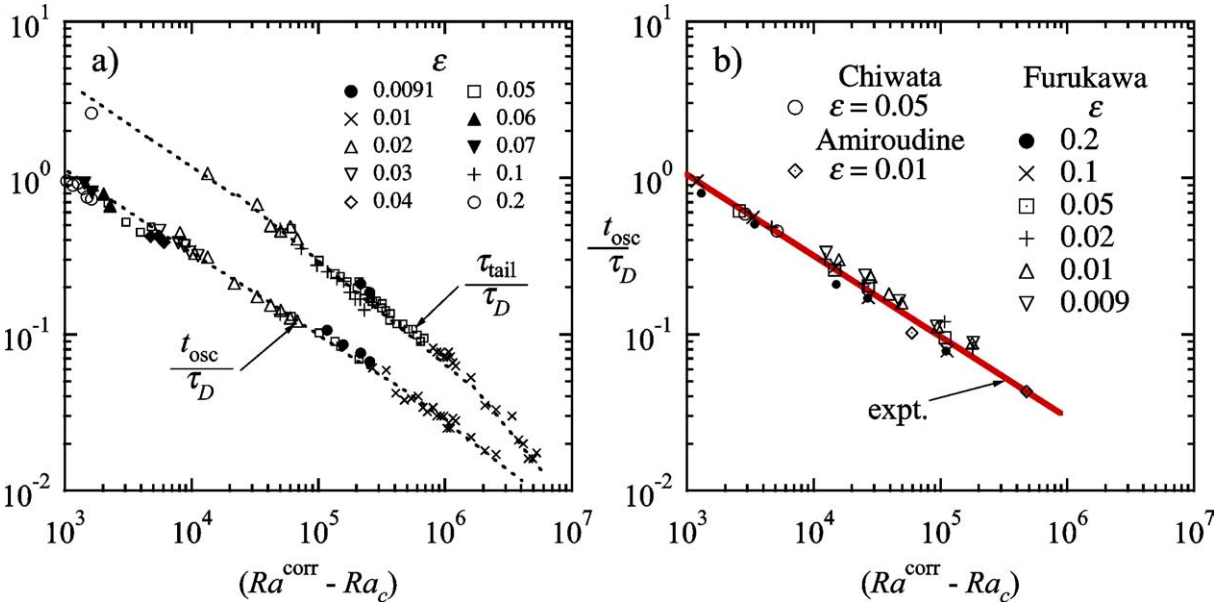

Fig. 10. The oscillation period $t_{\rm osc}$ and the relaxation time $\tau_{\rm tail}$ to the steady-state, both scaled by the diffusion time τ_D, versus $[Ra^{\rm corr} - Ra_c]$. (a) Experimental data at various values of ε. (b) Symbols show the data from simulations at different values of ε, the solid line is the average of the experimental data in (a). Taken from [36]. (Figure initially published by the American Physical Society.)

Fig. 10. Période d'oscillation $t_{\rm osc}$ et le temps de relaxation $\tau_{\rm tail}$ pour atteindre l'état stationnaire, tous deux rapportés au temps de diffusion τ_D, en fonction de $[Ra^{\rm corr} - Ra_c]$. (a) Résultats expérimentaux pour plusieures valeurs de ε. (b) Les symboles montrent les résultats des simulations numériques pour différentes valeurs de ε, et la ligne continue est la moyenne des résultats expérimentaux dans la partie (a). D'après [36]. (Figure initialement publiée par l'American Physical Society.)

In Fig. 8, we show two representative temperature profiles $\Delta T(t)$ for ^{3}He along the critical isochore. For $\varepsilon = 0.01$, the simulations by Amiroudine and Zappoli [34] are compared with the experimental data [30], and for $\varepsilon = 0.05$ the comparison of the data is with the simulations by Chiwata and Onuki [32]. Both experiments and simulations exhibit remarkable damped oscillations which are not observed in the transient of a similar experiment in a liquid at constant pressure [29]. The oscillations can be explained by the mechanism of the piston effect as described in [34] and [33]. Briefly, as the fluid becomes mechanically destabilized during the initial increase of $\Delta T(t)$ with time, plumes are formed and produce a 'cold' boundary layer at the top plate. This triggers a piston effect which causes a homogeneous decrease of the bulk temperature. This in turn induces a decrease of the temperature gradient in the cold boundary layer, and which is seen as a decrease in $\Delta T(t)$. As a result, the cold piston effect is weakened and a hot piston effect arises due to the heating of the bottom wall. Then a new warming cycle begins with an increase of the bulk temperature. The resulting minimum, and the subsequent damped oscillatory profile leads to steady-state convection with the final value ΔT.

Both the experimental results [30] and the simulation data [36] of the steady-state $\Delta T(q, \varepsilon)$ could be represented in a scaled form over a range of ε where the compressibility varied by a factor of about 30. This was done in terms of the dimensionless convection heat current $j^{\rm conv}_{\rm corr} \propto Ra_{\rm corr}(Nu_{\rm corr} - 1)$, which was plotted versus $ra^*_{\rm corr} \equiv (Ra_{\rm corr} - Ra_c)/Ra_c$ [30]. Here, for the purpose of a more sensitive representation, the ratio $j^{\rm conv}_{\rm corr}/ra^*_{\rm corr}$ is plotted versus $ra^*_{\rm corr}$, as shown in Fig. 9. Furukawa and Onuki [33] theoretically justified the validity of the scaling in terms of the corrected Ra and Nu. Similarly the periods $t_{\rm osc}$ between the succeeding minima in the damped oscillations for the various values of q and ε could be cast into a scaled plot $t_{\rm osc}/\tau_D$ versus $(Ra_{\rm corr} - Ra_c)$, where τ_D is the diffusive relaxation time which is proportional to τ_0, defined in Eq. (6). Simulations [34,36] and experimental results are in quite good agreement, as shown in Fig. 10 but this scaling still needs a theoretical justification.

These positive results should stimulate further research in numerical simulation aimed at resolving systematic discrepancies in the transient of $\Delta T(t)$ which appear to increase with ε and with decreasing $(Ra_{\text{corr}} - Ra_c)$, and increase with ε, as described in [36].

4. Conclusions

As can be judged from the few examples presented in Section 2, the equilibration phenomena of fluids near the critical point are now quite well understood, which is an important consideration for further experiments under μg conditions. On the other hand, non-linear phenomena in compressible fluids are more complicated to describe. Theory and simulation for steady conditions for convection in a RB cell have greatly progressed recently [2] and this is reflected by the comparison between simulations and experiments. For the transients to steady-state convection, 2D simulations reproduce the damped oscillations reported in the experiments. However there are systematic discrepancies, and some aspects of the observed $\Delta T(t)$ are not reproduced in the simulations. Resolving these open questions poses a challenge and more simulations, possibly in 3D, need to be considered.

Acknowledgements

We dedicate this review to R.F. Berg and M.R. Moldover, the organizers of the 1989 workshop. For the introductory remarks in Section 2 we have been guided by the presentation in the PhD thesis of A. Kogan, Duke University (2000), and wish to acknowledge his contribution. This work has been supported by NASA Grant NAG3-1838.

References

[1] Equilibration Near the Critical Point, Workshop held at the National Institute of Standards and Technology (NIST), Gaithersburg, MA, March 16–17, 1989, R.F. Berg, M.R. Moldover, Chairs of Organizing Committee.
[2] B. Zappoli, C. R. Mécanique 331 (2003) 713.
[3] K. Nitsche, J. Straub, in: Proceedings of the Sixth European Symposium on Material Sciences under Microgravity Conditions, Bordeaux, France, 1986 (European Space Agency, Paris), vol. SP-256, 1987, p. 109;
See also J. Straub, K. Nitsche, Fluid Phase Equilibria 88 (1993) 183.
[4] J. Straub, A. Haupt, L. Eicher, Int. J. Thermophys. 16 (1995) 1033.
[5] C. Pittman, L. Cohen, H. Meyer, J. Low Temp. Phys. 46 (1982) 115.
[6] A. Onuki, H. Hao, R.A. Ferrell, Phys. Rev. A 41 (1990) 2256.
[7] A. Onuki, R.A. Ferrell, Physica A 164 (1990) 245.
[8] H. Boukari, J.N. Shaumeyer, M.E. Briggs, R.W. Gammon, Phys. Rev. A 41 (1990) 2260.
[9] B. Zappoli, D. Bailly, Y. Garrabos, B. Le Neindre, P. Guenoun, D. Beysens, Phys. Rev. A 41 (1990) 2264.
[10] R.P. Behringer, A. Onuki, H. Meyer, J. Low Temp. Phys. 81 (1990) 71.
[11] B. Zappoli, Phys. Fluids 4 (1992) 1040.
[12] J. Straub, L. Eicher, A. Haupt, Phys. Rev. E 51 (1995) 5556;
J. Straub, L. Eicher, A. Haupt, Int. J. Thermophys. 16 (1995) 1051.
[13] H. Boukari, R.L. Pego, R.W. Gammon, Phys. Rev. E 52 (1995) 1614.
[14] H. Boukari, M.E. Briggs, J.N. Shaumeyer, R.W. Gammon, Phys. Rev. Lett. 65 (1990) 2654.
[15] P. Guenoun, B. Khalil, D. Beysens, Y. Garrabos, F. Kammon, B. Le Neindre, B. Zappoli, Phys. Rev. E 47 (1993) 1531.
[16] F. Zhong, H. Meyer, Phys. Rev. E 51 (1995) 3223.
[17] A.B. Kogan, H. Meyer, J. Low Temp. Phys. 112 (1998) 419.
[18] F. Zhong, A. Kogan, H. Meyer, J. Low Temp. Phys. 108 (1997) 161.
[19] F. Zhong, H. Meyer, J. Low Temp. Phys. 114 (1999) 231.
[20] R.A. Wilkinson, G.A. Zimmerli, H. Hao, M.R. Moldover, R.F. Berg, W.L. Johnson, R.A. Ferrell, R.W. Gammon, Phys. Rev. E 57 (1998) 436.

[21] F. Zhong, H. Meyer, Phys. Rev. E 53 (1996) 5935.
[22] R. Wunenburger, Y. Garrabos, C. Lecoutre-Chabot, D. Beysens, J. Hegseth, Phys. Rev. Lett. 84 (2000) 1400.
[23] R. Wunenburger, Y. Garrabos, C. Lecoutre, D. Beysens, J. Hegseth, F. Zhong, M. Barmatz, Int. J. Thermophys. 23 (2002) 103.
[24] A. Haupt, J. Straub, Phys. Rev. E 59 (1999) 1795.
[25] M. Gitterman, V. Steinberg, J. Appl. Math. Mech. USSR 34 (1971) 305;
M. Gitterman, Rev. Mod. Phys. 50 (1978) 85.
[26] P. Carlès, B. Ugurtas, Physica D 126 (1999) 69.
[27] L.D. Landau, E.M. Lifshitz, Course of Theoretical Physics, vol. 6, Fluid Mechanics, Pergamon, Oxford, 1959.
[28] D.J. Tritton, Physical Fluid Dynamics, Oxford Science, Oxford, 1988, Section 14.6.
[29] R.P. Behringer, Rev. Mod. Phys. 57 (1985) 657.
[30] A.B. Kogan, H. Meyer, Phys. Rev. E 63 (2001) 056310.
[31] H. Meyer, A.B. Kogan, Phys. Rev. E 66 (2002) 056310.
[32] Y. Chiwata, A. Onuki, Phys. Rev. Lett. 87 (2001) 144301.
[33] A. Furukawa, A. Onuki, Phys. Rev. E 66 (2002) 016302.
[34] S. Amiroudine, B. Zappoli, Phys. Rev. Lett. 90 (2003) 105303;
S. Amiroudine, private communication.
[35] L. El Khouri, P. Carlès, Phys. Rev. E 66 (2002) 066309.
[36] A. Furukawa, H. Meyer, A. Onuki, A.B. Kogan, Phys. Rev. E 68 (2003) 056309.